J Mater Sci (2011) 46:4377–4383
DOI 10.1007/s10853-011-5323-0

IIB 2010

Indium adsorption and incorporation mechanisms in AlN

Efterpi Kalesaki · Joseph Kioseoglou · Philomela Komninou · Theodoros Karakostas

Received: 31 August 2010 / Accepted: 24 January 2011 / Published online: 5 February 2011

Abstract Density functional theory calculations are implemented in order to scrutinize indium adsorption and incorporation mechanisms in polar AlN. Indium adsorption is promoted on both polarity surfaces and adatom kinetics calculations indicate lower diffusion barriers of indium along the prismatic $\langle 11\bar{2}0\rangle$ directions on (0001) as well as $(000\bar{1})$ AlN. The latter is correlated to experimental observations of $In_{0.24}Al_{0.76}N$ grown by metal organic vapour phase epitaxy, demonstrating indium concentration along the facet junctions of V-defects. This can be attributed to In surface diffusion along the $\langle 11\bar{2}0\rangle$ directions of the pyramidal facets. Surface thermodynamics reveal a manifold behaviour of indium in polar AlN surfaces, significantly affected by polarity, growth stoichiometry as well as surface termination. In particular, N-rich growth conditions enhance indium incorporation on Al-terminated surfaces of both polarities, leading up to full monolayer coverage. Incorporation on N-terminated (0001) and $(000\bar{1})$ surfaces is hindered independent of growth stoichiometry.

Introduction

Ternary $In_xAl_{1-x}N$ thin films are acknowledged as high potential structures for optoelectronic and high-power electronic applications [1]. However, growth of InAlN is a profound issue due to the large difference in covalent bonds and growth temperatures of its constituent materials. The intricate nature of InAlN growth is further demonstrated by recent experimental observations on metal–organic vapour phase epitaxy (MOVPE) [2, 3] and molecular beam epitaxy (MBE) [4, 5] grown InAlN thin films of various concentrations, which indicate diverse growth mechanisms.

In order to attain high quality epitaxial layers, their surface morphology must be thoroughly controlled. The surface formation energy is sufficient to define the morphology if growth is performed under thermodynamic equilibrium. However, if growth is performed under non-equilibrium conditions, kinetic effects become important and identification of the adatom kinetics, the corresponding diffusion barriers and migration pathways becomes imperative. While surface adatom kinetics are a key parameter in optimizing the surface morphology and the overall material quality, experimental methods are insufficient in accurately monitoring the diffusion process. Hence theoretical calculations are established as an indispensable tool towards growth optimization [e.g. 6].

In the current study, a comprehensive theoretical analysis is applied in order to clarify the optimum structural characteristics and growth conditions, in particular growth stoichiometry (III/V ratio), promoting In adsorption and incorporation in polar AlN surfaces. In that manner, we aim to provide valuable feedback in growth optimization of InAlN alloys as well as InN/AlN heterostructures. Density functional theory (DFT) calculations are accomplished in order to identify the favourable adsorption sites for indium adatoms and the corresponding diffusion barriers following previous calculations on polar III-Nitride surfaces [7, 8]. Moreover incorporation of indium in polar AlN surfaces is studied, considering In as a substitutional atom [e.g. 9], and taking into account polarity, surface termination as well as stoichiometry.

The calculations distinguish the minimum energy lattice sites assisting In adsorption. Migration paths equivalent to

E. Kalesaki · J. Kioseoglou · P. Komninou (✉) · T. Karakostas
Department of Physics, Aristotle University of Thessaloniki, 54124 Thessaloniki, Greece
e-mail: komnhnoy@auth.gr

the $\langle 11\bar{2}0\rangle$ are perceived in agreement with the experimental observations on MOVPE InAlN thin films. N-rich growth conditions are predicted to promote indium incorporation on Al-terminated surfaces of both polarities, leading up to full monolayer coverage. In contrast, indium incorporation is prevented in N-terminated (0001) and $(000\bar{1})$ AlN independent of stoichiometry.

Computational details and the implemented methodology are described in "Computation method" section. The results on In adsorption and incorporation are discussed in detail in "Indium adsorption on polar AlN surfaces" and "Indium incorporation in polar AlN surfaces" sections, respectively. Finally the conclusions are summarized in "Conclusions" section.

Computation method

The adsorption and incorporation of In on polar AlN surfaces were investigated by first principles calculations, exploiting a slab geometry methodology in order to distinguish Al- and N-polar surfaces, also denoted as (0001) and $(000\bar{1})$, respectively. Conventionally the [0001] direction in such polar structures is considered parallel to the Al–N bonds along the c axis. Hence the two different polarities are distinguished by the orientation of the Al–N bonds; if the Al–N bond points upwards the layer is Al-polar whereas if it points downwards it is N-polar. Total energy values were determined by DFT calculations employing the Perdew–Burke–Ernzehof (PBE) generalized gradient approximation (GGA) [10] in the VIENNA ab initio simulation package (VASP) [11, 12]. Projector augmented-wave pseudopotentials [13] were implemented and the indium *4d* electrons were included in the valence. The equilibrium lattice constants and internal parameter u of AlN were $a = 3.1265$ Å, $c = 5.0355$ Å, $u = 0.3785$ in fair agreement to previous experimental values [14].

The band gap underestimation by the most popular DFT approximations, namely GGA and the local density approximation (LDA), is currently extensively discussed. Interest is primarily focused on its effect on the calculated formation energies and most importantly possible techniques to overcome this problem. Various approaches, e.g. screened exchange LDA (sX-LDA), LDA/GGA including a Hubbard-U term (LDA/GGA+U) or self-interaction corrections, the GW approximation and hybrid functional calculations, are investigated in order to accurately calculate the formation energies of point defects with DFT (e.g. [15–17] and references therein). However, these approaches are still under investigation and integrated total energy calculations have only been performed in specific material systems. Furthermore such errors could be eliminated, under implementation of LDA/GGA, when total energy differences are considered.

In the current study, surfaces were treated using 3×3 AlN slabs comprising five Al–N double layers. The plane wave cut-off energy was 50 Ry and the Brillouin zone was sampled by a $4 \times 4 \times 1$ k-point grid. The bottom surface of the investigated slab configurations was passivated by fractionally charged pseudohydrogens, having charge 3/4 and 5/4 for N and Al atoms, respectively. A vacuum region equal to 12 Å along [0001] was used. Atoms on the upper three bilayers were allowed to relax, while the bottom two bilayers and the corresponding pseudohydrogens were kept fixed, after having their positions already optimized in a first relaxation step.

In general, the formation energy of a defect system is given by [e.g. 18]:

$$E_{\mathrm{f}} = E_{\mathrm{D}}^{\mathrm{tot}} - E_{\mathrm{bulk}}^{\mathrm{tot}} + \sum_i n_i \mu_i + q(E_{\mathrm{v}} + E_{\mathrm{F}}) \quad (1)$$

where $E_{\mathrm{D}}^{\mathrm{tot}}$is the total energy of a supercell comprising the defect in a charge state q and $E_{\mathrm{bulk}}^{\mathrm{tot}}$ is the total energy of the equivalent, reference supercell i.e. the corresponding ideal crystal. The term n_i indicates the number of atoms of type i, host or impurity atoms, added ($n_i \succ 0$) or removed ($n_i \prec 0$) from the reference supercell. The term μ_i corresponds to the chemical potential of the ith element. In Eq. 1, the term E_{v} is the energy at the valence band maximum of the ideal crystal and E_{F} is the Fermi energy relative to E_{v}. In this study, indium atoms are considered to be in a neutral charge state, i.e. $q = 0$. In "Indium adsorption on polar AlN surfaces" section, relative energies are presented on the adsorption of a single indium atom in various lattice sites of equally sized supercells. In particular, the formation energy differences of the considered reconstructions are given, which are equal to their total energy differences according to Eq. 1. Hence, as previously discussed, terms corresponding to band gap corrections are eliminated. In the second part ("Indium incorporation in polar AlN surfaces" section), we focus on the incorporation of a single, indium atom in the topmost and subsurface layers of AlN as well as on the incorporation of multiple indium atoms in the topmost surface layer, discarding band gap correction terms in the latter case. The presented energy values, following Eq. 1 are calculated by:

$$\Delta E = \Delta \mathrm{E}_{\mathrm{tot}} + n_{\mathrm{Al}}\mu_{\mathrm{Al}} + n_{\mathrm{In}}\mu_{\mathrm{In}} \quad (2)$$

where $\Delta \mathrm{E}_{\mathrm{tot}} = E_{\mathrm{D}}^{\mathrm{tot}} - E_{\mathrm{bulk}}^{\mathrm{tot}}$, having as reference the relaxed, ideal crystal; (0001) and $(000\bar{1})$ AlN surfaces being either Al- or N-terminated. In Eq. 2, n_i (i = Al, In) is either negative or positive depending on whether Al/In atoms are removed or put into the model, respectively.

Results and discussion

Indium adsorption on polar AlN surfaces

The minimum energy positions for indium adatoms on the Al-terminated (0001) and N-terminated (000$\bar{1}$) AlN surfaces were investigated, considering full relaxation of the adatoms and the surface atoms (upper three bilayers). The 'hcp', 'fcc', 'bridge' and 'top' lattice sites [7] were examined as distinct adsorption sites. Indium adatoms with a 'bridge' or 'fcc' starting position relaxed towards the 'hcp' lattice site on the (0001) surface (Fig. 1a). Likewise indium adatoms with a 'bridge' starting position relaxed towards the 'fcc' lattice site on the (000$\bar{1}$) surfaces (Fig. 1b). Thus, the minimum and maximum energy positions were unambiguously identified for each polarity; 'hcp' and 'fcc' sites as most stable for (0001) and (000$\bar{1}$) surfaces, respectively and 'top' positions as highly unfavourable in both cases. In Fig. 1a, relative energies are presented having as reference the 'hcp' position, which has an energy difference of -0.615 eV/Å^2 (III-rich) and -0.726 eV/Å^2 (N-rich) with respect to unreconstructed (0001) surfaces. For (000$\bar{1}$) surfaces (Fig. 1b) relative energies of the investigated reconstructions with respect to the 'fcc' position are presented. Energy differences equal to -0.179 eV/Å^2 (III-rich) and -0.289 eV/Å^2 (N-rich) were obtained for the 'fcc' with respect to unreconstructed (000$\bar{1}$) surfaces.

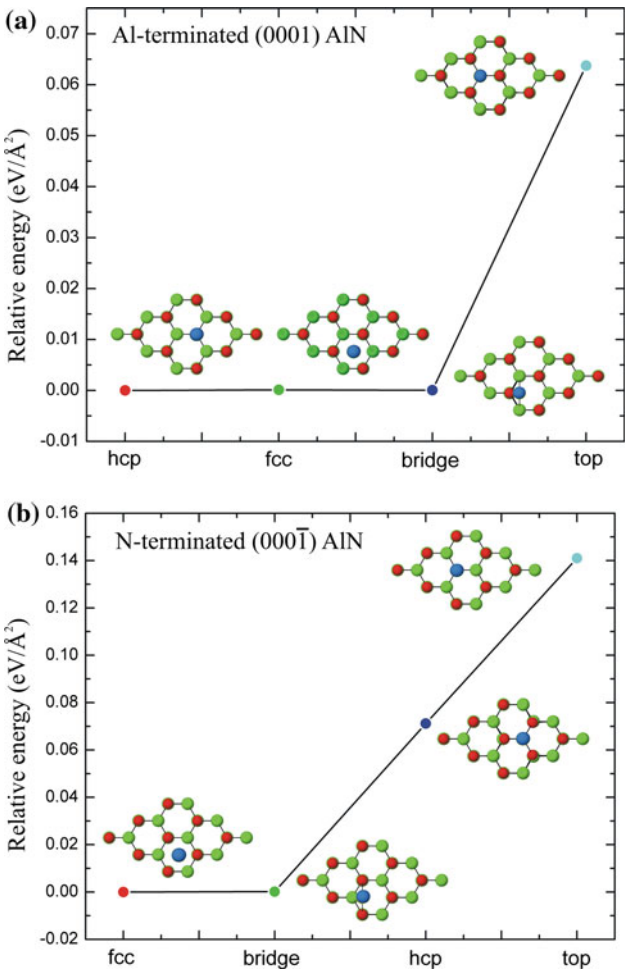

Fig. 1 Relative energies of In adsorption on the 'hcp', 'fcc', 'bridge' and 'top' lattice sites of Al-terminated (0001) (**a**) and N-terminated (000$\bar{1}$) (**b**) AlN surfaces (top views of the initial configurations are given as *insets*). The energetically most stable reconstructions with respect to the unreconstructed AlN surfaces are used as reference in each case, i.e. the 'hcp' for (0001) and the 'fcc' for (000$\bar{1}$) AlN surfaces. In the former case, the 'fcc' and 'bridge' starting positions relaxed towards the 'hcp' while in the latter the 'bridge' reconstruction relaxed towards the 'fcc'. Al atoms are illustrated as *green* (*light coloured/larger*), In atoms as *blue* (*dark coloured/larger*) and N atoms as *red* (*dark coloured/smaller*) spheres (Color figure online)

The surface kinetics of adsorbed In atoms, their migration pathways and diffusion barriers were studied by potential energy surface (PES) calculations. Surface atoms and In adatoms were fixed laterally in position and were only allowed to relax normal to the surface. PES calculations reveal that in the case of (0001) AlN, the 'hcp' lattice site is energetically favourable, in agreement to the previous calculation. The 'bridge' lattice sites are metastable positions while occupation of a 'top' lattice site, where the In adatom forms a single bond, results in barriers of 0.0846 eV/Å^2 (Fig. 2a, b) with respect to the energetically favourable 'hcp' lattice site. Indium is predicted to migrate through the 'fcc' lattice sites in order to reside on top of an underlying N atom ('hcp' site) since minimum diffusion barriers equal to 0.055 eV/Å^2 are observed from the 'hcp' towards the 'fcc' position.

In (000$\bar{1}$) surfaces the pathway of In adatoms is also delimited by the 'fcc' and 'hcp' lattice sites; the former corresponding to a global while the latter to a local minima as illustrated in Fig. 3. The 'bridge' lattice sites are identified as metastable positions and occupation of a 'top' lattice site, where the In adatom forms a single bond, results in a barrier of 0.1336 eV/Å^2 with respect to the energetically favourable 'fcc' lattice site. Hence diffusion of In atoms to 'fcc' lattice sites through the 'hcp' position is most likely to occur. The corresponding diffusion barrier is calculated at 0.0165 eV/Å^2. It is thus evident that adsorption is overall promoted on lattice sites ('fcc' and 'hcp') where In adatoms shall form the maximum number of bonds.

Both PES calculations of Figs. 2 and 3, lead to identical migration paths of indium on the two polarity surfaces. Indium adatoms diffuse through the hcp–bridge–fcc sites and vice versa. These migration components establish the In diffusion path on polar AlN surfaces along the $\langle 11\bar{2}0 \rangle$ directions (Fig. 4).

Experimental evidence on the diffusion paths of indium atoms was provided in Ref. [2]. High-resolution Z-contrast

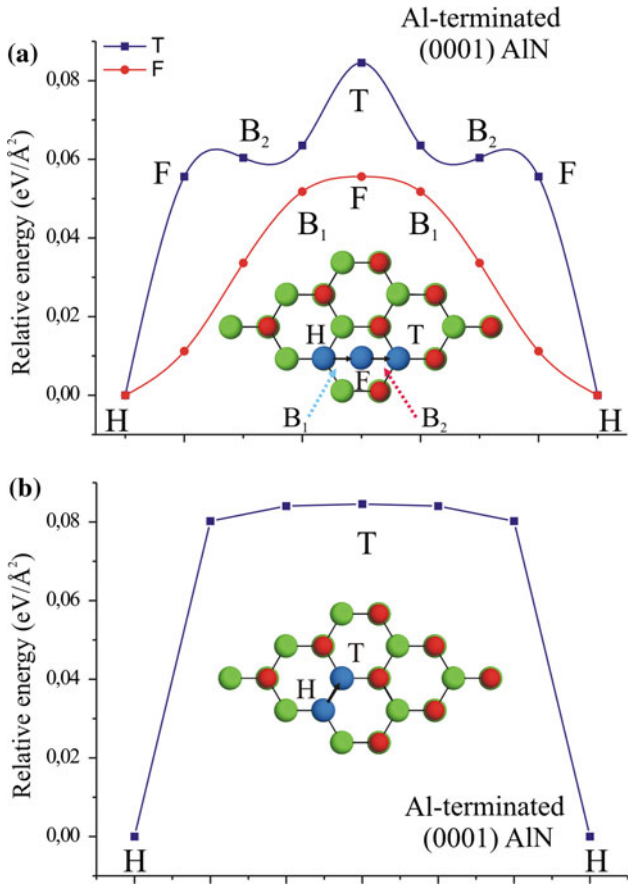

Fig. 2 **a** Calculated relative energies along the hcp (H)-bridge(1) (B_1)-fcc (F) and hcp (H)-fcc (F)-bridge(2) (B_2)-top (T) migration pathways on Al-terminated (0001) AlN surfaces including the values of the intermediate sites taken into consideration. The relaxed ideal supercell is presented in top view and the investigated pathways are denoted by *solid arrows*. The two distinct B sites (B_1 and B_2), differentiating on the bonding environment of the indium atom, are indicated by *discontinuous arrows*. In **b** the calculated relative energies along the alternative diffusion path of indium from hcp (H) directly to the top (T) position considering two intermediate sites is also presented. This direct transition is indicated by a *solid black arrow*. Ball and stick models are illustrated in accordance to Fig. 1

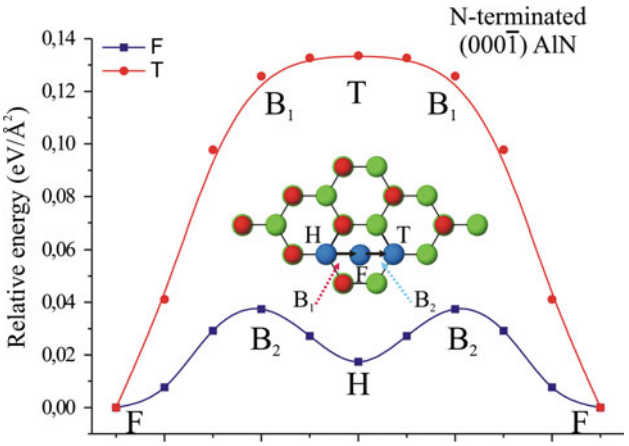

Fig. 3 Calculated relative energies along the fcc (F)-bridge(1) (B1)-hcp (H) and fcc (F)-bridge(2) (B2)-top (T) migration pathways on N-terminated (000$\bar{1}$) AlN surfaces including the values of the intermediate sites taken into consideration. The relaxed ideal supercell is presented in top view and the investigated pathways are denoted by *solid arrows*. The two distinct B sites (B1 and B2), differentiating on the bonding environment of the indium atoms, are indicated by *discontinuous arrows*. Illustrations are as in previous figures

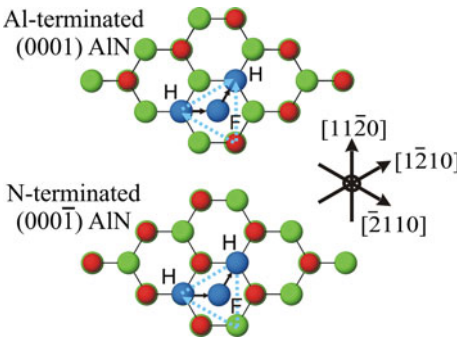

Fig. 4 Surface diagrams depicting the diffusion paths of In adatoms on Al-terminated (0001) and N-terminated (000$\bar{1}$) AlN surfaces, identified as the ⟨11$\bar{2}$0⟩ directions. Ball and stick models are illustrated in accordance to Fig. 1

images of V-defects in MOVPE $In_{0.24}Al_{0.76}N$ clearly showed an enhanced occurrence of indium at particular crystallographic directions and sites, i.e. the prismatic ⟨11$\bar{2}$0⟩ directions on polar InAlN surfaces and along their projections on the {10$\bar{1}$1} sidewalls facets of the V-defects as shown in Fig. 5. The latter provides a justification of the In adatom kinetics calculations identifying the ⟨11$\bar{2}$0⟩ directions as the minimum energy diffusion paths.

Indium incorporation in polar AlN surfaces

In addition to Indium adsorption, total energy calculations of In incorporation on polar AlN surfaces were accomplished. As previously discussed, (0001) and (000$\bar{1}$) supercells are distinguished by the orientation of the III-N bond. Nevertheless, an Al-terminated (0001) supercell will retain its sense of polarity if the topmost Al atoms are removed. The same stands for N-terminated (000$\bar{1}$) surfaces if the topmost N atoms are taken out from the supercell [e.g. 19]. Hence two distinct cases may be considered for each polarity; Al(N)-polar material being either Al- or N-terminated.

In the diagram of Fig. 6, the relative stability ($\Delta E_{Al-Ntermination}$) of the considered surface terminations for each polarity is presented as a function of the Al chemical potential (μ_{Al}) and consecutively of growth stoichiometry.

For (0001) surfaces, the energy difference of the two possible terminations is $\Delta E_{Al-Ntermination} = E_{tot}^{Al-termination} - E_{tot}^{N-termination} + n_{Al}\mu_{Al}$ while for (000$\bar{1}$) the equation is

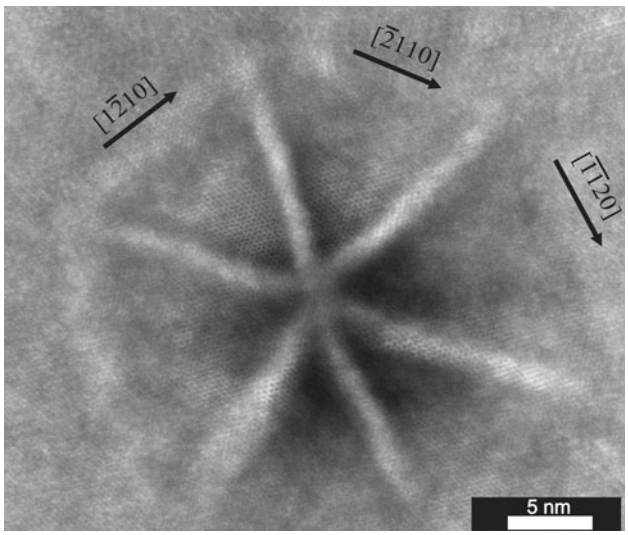

Fig. 5 High-resolution Z-contrast STEM image revealing high In concentration along the $\langle 11\bar{2}0\rangle$ directions on the MOVPE InAlN surface and the $\{10\bar{1}1\}$ sidewalls facets of the V-defects. Darker contrast is observed away from these directions

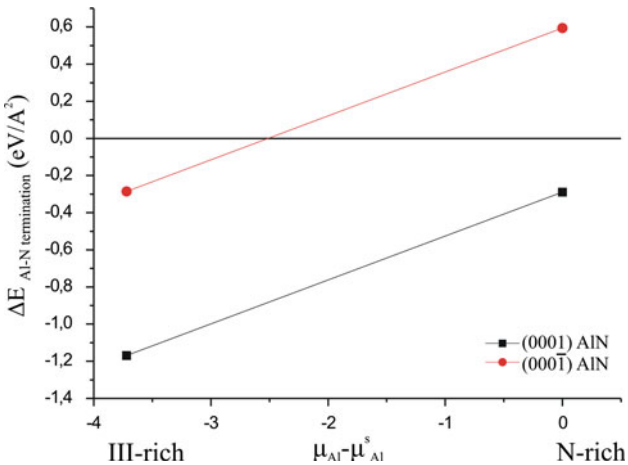

Fig. 6 Relative energies ($\Delta E_{Al-Ntermination}$) of Al- and N-terminated surfaces in eV/Å^2 for (0001) (*black-darker line/square symbols*) and (000$\bar{1}$) (*red-lighter line/circular symbols*) AlN surfaces as a function of the Al chemical potential μ_{Al}. The term μ^s_{Al} corresponds to the chemical potential of solid Al (Color figure online)

$\Delta E_{Al-Ntermination} = E^{Al-termination}_{tot} - E^{N-termination}_{tot} + n_N\mu_N$ where $E_{tot}$is the total energy of each possible termination and n_{Al},n_N correspond to Al, N atoms respectively with $n_{Al} \prec 0$ and $n_N \succ 0$. The chemical potentials of Al, N are expressed as:

$$\mu_{Al} = \mu^s_{Al} + (1-\lambda)\Delta H^f_{AlN} \quad (3)$$

$$\mu_N = \mu_{AlN} - \mu_{Al} \quad (4)$$

if we consider Al and N atoms in thermodynamic equilibrium with AlN.

In the above equations μ^s_{Al} is the chemical potential of solid Al, ΔH^f_{AlN} the formation enthalpy of AlN and μ_{AlN} refers to bulk AlN. The term λ depends on the growth stoichiometry and is $0(N-\text{rich}) \leq \lambda \leq 1(III-\text{rich})$. We thus consider an upper (μ^s_{Al} for III-rich) and a lower ($\mu^s_{Al} + \Delta H^f_{AlN}$ for N-rich) limit of the Al chemical potential. In these two extremes, AlN shall be unstable against the formation and desorption of N_2 molecules (N-rich) or against the formation of Al droplets (III-rich) (for further details see e.g. 19). Eq. 3 designates the Al chemical potential as a linear function of the AlN formation enthalpy. Thus, the energy difference $\Delta E_{Al-Ntermination}$ varies linearly with μ_{Al} between the two extreme cases of $\mu_{Al} = \mu^s_{Al} + \Delta H^f_{AlN}$ and $\mu_{Al} = \mu^s_{Al}$ for N and III-rich growth conditions, respectively (Fig. 6).

It is overall evident that the metal rich termination of the (0001) surfaces is highly stable independent of growth conditions. In the case of (000$\bar{1}$) AlN, III-rich growth promotes metal termination. However, N-terminated (000$\bar{1}$) surfaces may also be formed under N-rich conditions. The latter cannot be excluded for (0001) surfaces and extensive areas of N-terminated material may be formed under extreme N-rich growth due to the small energy difference between Al and N surface terminations.

First, the relative stability of configurations comprising a single In atom in different layers of the investigated slabs was examined. Calculations point to preferential In incorporation on the topmost layer of Al-terminated (0001) surfaces independent of growth conditions (Fig. 7(a)) while reconstructions comprising an indium atom in deeper layers are stabilized under N-rich growth. In contrast incorporation in N-terminated (0001) surfaces is hindered. Energy differences of 0.341, 0.358 and 0.364 eV/Å^2 to the equivalent, ideal (0001) AlN surfaces were calculated for incorporation on the first, second and third layers under III-rich conditions, respectively. The corresponding values, considering N-rich growth, were equal to 0.027, 0.044 and 0.049 eV/Å^2 indicating significantly lower barriers for In incorporation.

In the case of Al-terminated (000$\bar{1}$) surfaces, In is preferentially incorporated on the topmost layer but it will not be stabilized in deeper layers even under N-rich conditions (Fig. 7b). Similar to N-terminated (0001) surfaces, N-terminated (000$\bar{1}$) surfaces hinder incorporation of In atoms. Energy differences of 0.315, 0.334 and 0.346 eV/Å^2 to the equivalent, ideal (000$\bar{1}$) AlN surfaces were calculated for incorporation on the first, second and third layers under III-rich conditions, respectively. The corresponding values, considering N-rich growth, were equal to 0.001, 0.019 and 0.031 eV/Å^2. The above results indicate that In prefers to reside on the surface of AlN rather than be incorporated in the bulk.

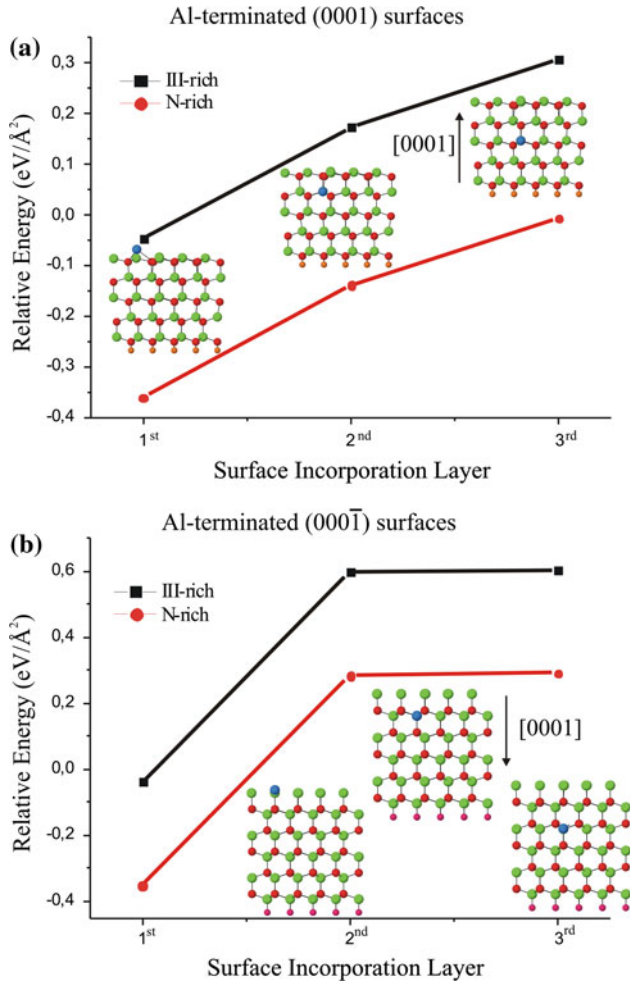

Fig. 7 Relative energies of Al-terminated (0001) (**a**) and (000$\bar{1}$) (**b**) AlN surfaces considering incorporation of In on subsequent layers of the investigated slab configurations, for III-rich and N-rich growth conditions. On Al-terminated (0001) surfaces incorporation is sensitive to the growth conditions: Promoted up to the third subsurface layer under N-rich growth while restricted on the topmost surface layer for III-rich conditions. In contrast, in the case of (000$\bar{1}$) surfaces incorporation on the topmost layer is energetically favourable independent of growth conditions. The energy of the corresponding ideal, relaxed AlN surface is used as reference in each case. In the relaxed structural models given as *inset*, Al, N and In atoms are illustrated as *green* (*light coloured/larger*), *red* (*dark coloured/smaller*) and *blue* (*dark coloured/larger*) spheres respectively. The dangling bonds on the bottom surface of the slabs are passivated by pseudohydrogens illustrated as *smaller orange* and *pink spheres* for (0001) and (000$\bar{1}$) surfaces, respectively (Color figure online)

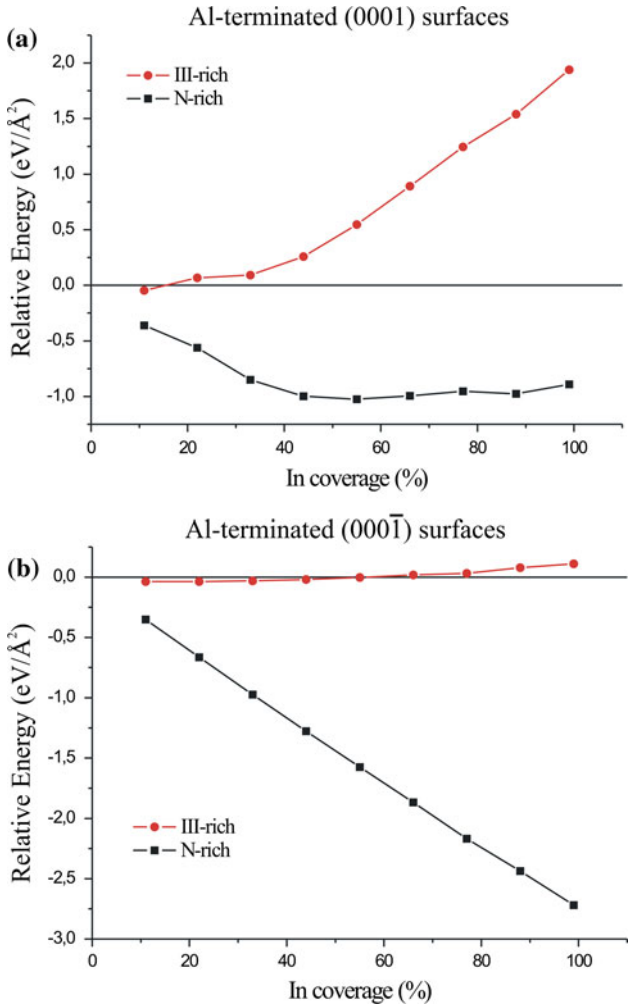

Fig. 8 Relative energies in eV/Å^2 of Al-terminated (0001) (**a**) and Al-terminated (000$\bar{1}$) (**b**) surfaces varying the indium coverage from zero to full monolayer, i.e. comprising nine indium atoms on the topmost surface layer. In each case, the energy of the ideal, relaxed AlN surface is used as reference

Second, calculations to Al-terminated reconstructions of both polarities comprising higher indium concentrations in the top surface layer were undertaken. As observed in Fig. 8a, incorporation in Al-terminated (0001) surfaces is constrained to a single indium atom under III-rich growth while N-rich conditions enhance indium incorporation and up to full monolayer coverage may be achieved. Full monolayer coverage is also predicted on Al-terminated (000$\bar{1}$) surfaces under N-rich growth as illustrated in Fig. 8b. However, in that latter case an In coverage of ~55% could be also achieved under III-rich conditions.

These results may be correlated with previous experimental observations on quaternary MBE grown AlGaInN where higher Al mole fractions were found to significantly lower In incorporation [20]. Overall the critical parameter in order to ensure enhanced In coverage on polar AlN surfaces is the implementation of N-rich growth conditions. The latter elucidates earlier experimental observations on ternary MBE InGaN [21, 22] where N-rich conditions were identified as necessary in order to achieve efficient In incorporation. This behaviour may be attributed to the higher strength of Al–N bonds in comparison to In-N, which is established by the corresponding cohesive energies of AlN (−11.669 eV) and InN (−7.97 eV) [e.g. 23 and references therein]. As a consequence, bonding of the

available active nitrogen to Al atoms is promoted under metal rich conditions. Conversely, under N-rich conditions the increased amount of nitrogen atoms enhances the In-N bonding probability, leading to films with higher InN mole fraction.

Conclusions

Density functional theory calculations were accomplished in order to investigate indium adsorption and incorporation in polar AlN. The optimum lattice sites for In adsorption on (0001) and $(000\bar{1})$ surfaces are identified and PES calculations reveal lower diffusion barriers along $\langle 11\bar{2}0\rangle$ for indium adatoms on both polarity surfaces, elucidating the diffusion of indium along the prismatic $\langle 11\bar{2}0\rangle$ directions as has been recently shown experimentally [2]. The polarity of the AlN surfaces and growth stoichiometry are identified as critical conditions, affecting indium incorporation significantly. N-rich conditions are established as a prerequisite in order to enhance indium incorporation on Al-terminated (0001) surfaces. Furthermore up to full monolayer coverage is predicted on Al-terminated $(000\bar{1})$ surfaces under N-rich conditions while enhanced coverage is also feasible under III-rich growth. In contrast, indium incorporation is prevented on N-terminated surfaces of both polarities independent of stoichiometry. Hence we may deduce that in order to ensure enhanced indium content in InAlN grown on polar AlN surfaces, growth should be performed under N-rich growth conditions.

Acknowledgements This study was supported by EC under the contract MRTN-CT-2004-05583 (PARSEM) and the 7th European Framework Project DOTSENSE (Grant no. STREP 224212).

References

1. Morkoc H (2008) Handbook of nitride semiconductors and devices. Wiley-VCH, Berlin
2. Kehagias Th, Dimitrakopulos GP, Kioseoglou J, Kirmse H, Giesen C, Heuken M, Georgakilas A, Neumann W, Karakostas Th, Komninou Ph (2009) Appl Phys Lett 95:071905
3. Brown DF, Keller St, Mates TE, Speck JS, DenBaars SP, Mishra UK (2010) J Appl Phys 107:033509
4. Sahonta S-L, Dimitrakopulos GP, Kehagias Th, Kioseoglou J, Adikimenakis A, Iliopoulos E, Georgakilas A, Kirmse H, Neumann W, Komninou Ph (2009) Appl Phys Lett 95:021913
5. Zhou L, Smith DJ, McCartney MR, Katzer DS, Storm DF (2007) Appl Phys Lett 90:081917
6. Ruterana P, Albrecht M, Neugebauer J (2003) Nitride semiconductors handbook on materials and devices. Wiley-VCH, Berlin
7. Zywietz T, Neugebauer J, Scheffler M (1998) Appl Phys Lett 73:487
8. Jindal V, Shahedipour-Sandvik F (2009) J Appl Phys 105:084902
9. van de Walle CG, Neugebauer J (2004) J Appl Phys 95:3851
10. Perdew JP, Burke K, Ernzerhof M (1996) Phys Rev Lett 77:3865
11. Kresse G, Furthmuller J (1996) Comput Mater Sci 6:15
12. Kresse G, Furthmuller J (1996) Phys Rev B 54:11169
13. Kresse G, Joubert J (1999) Phys Rev B 59:1758
14. Strite S, Morkoc H (1992) J Vac Sci Technol B 10:1237
15. Lany St, Zunger A (2008) Phys Rev B 78:235104
16. Nieminen MR (2009) Model Simul Mater Sci Eng 17:084001
17. Lambrecht L. R. W. (2010) Phys Stat Sol (b) 1–12. doi: 10.1002/pssb.201046327
18. Persson C, Zhao Y-J, Lany S, Zunger A (2005) Phys Rev B 72:035211
19. Kioseoglou J, Kalessaki E, Dimitrakopulos GP, Komninou Ph, Karakostas Th (2008) J Mater Sci 43:3982. doi:10.007/s10853-007-2235-0
20. Monroy E, Gogneau N, Jalabert D, Bellet-Amalric E, Hori Y, Enjalbert F, Dang LS, Daudin B (2003) Appl Phys Lett 82:2242
21. Pau JL, Pereiro J, Rivera C, Munoz E, Calleja E (2005) J Cryst Growth 278:718
22. Averbeck R, Riechert H (1999) Phys Stat Sol (a) 176:301
23. Zoroddu A, Bernardini F, Ruggerone P, Fiorentini V (2001) Phys Rev B 64:045208